Analyst

Accepted Manuscript

ROYAL SOCIETY OF CHEMISTRY

www.rsc.org/analyst

Cite this: DOI: 10.1039/c0xx00000x

www.rsc.org/xxxxxx

ARTICLE TYPE

Monitoring UVR induced damage in single cells and isolated nuclei using SR–FTIR microspectroscopy and 3D confocal Raman imaging

Ewelina Lipiec[a,b], Keith R. Bambery[c], Philip Heraud[b,d], Wojciech M. Kwiatek[a], Don McNaughton[b], Mark J. Tobin[c], Christian Vogel [b,e], Bayden R. Wood [* b]

Received (in XXX, XXX) Xth XXXXXXXXX 20XX, Accepted Xth XXXXXXXXX 20XX

DOI: 10.1039/b000000x

SR-FTIR in combination with Principal Component Analysis (PCA) was applied to investigate macromolecular changes in a population of melanocytes and their extracted nuclei induced by environmentally relevant fluxes of UVR (Ultraviolet Radiation). Living cells and isolated cellular nuclei were investigated post-irradiation for three different irradiation dosages (130, 1505, 15052 Jm^{-2} UVR, weighted) after either 24 or 48 hours of incubation. DNA conformational changes were observed in cells exposed to an artificial UVR solar-simulator source as evidenced by a shift in the DNA asymmetric phosphodiester vibration from 1236 cm^{-1} to 1242 cm^{-1} in the case of the exposed cells and from 1225 cm^{-1} to 1242 cm^{-1} for irradiated nuclei. PCA Scores Plots revealed distinct clustering of spectra from irradiated cells and nuclei from non-irradiated controls in response to the range of applied UVR radiation doses. 3D Raman confocal imaging in combination with k-means cluster analysis was applied to study the effect of the UVR radiation exposure on cellular nuclei. Chemical changes associated with apoptosis were detected and included intra-nuclear lipid deposition along with chromatin condensation. The results reported here demonstrate the utility of SR-FTIR and Raman spectroscopy to probe in situ DNA damage in cell nuclei resulting from UVR exposure. These results are in agreement with the increasing body of evidence that lipid accumulation is a characteristic of aggressive cancer cells, and are involved in the production of membranes for rapid cell proliferation.

Introduction

Excessive exposure to ultraviolet radiation (UVR) in sunlight may result in DNA damage, which can cause skin cancer. The incidence of skin cancer has increased over the past decade. Globally, non–melanoma skin cancers afflict 2 – 3 million people per annum, while melanoma skin cancers account for 132,000 of these each year.[1] One in every three cancers diagnosed is a skin cancer. The highest risk group is white Caucasian people living in regions of higher solar flux such as Australia and the USA. Skin cancers account for 80% of all newly diagnosed cancers in Australia with two in three Australians diagnosed with skin cancer by the time they are 70.[2] General practitioners in Australia have over 1 million patient consultations per year for skin cancer and around 434,000 people are treated for one or more non–melanoma skin cancers.[3] According to the US Skin Cancer Foundation statistics, one in every five Americans will develop skin cancer in their lifetime.[4]

Many studies have shown that UV-A (ultraviolet–A: 320–400 nm) and UV-B (ultraviolet–B: 280–320 nm) components are responsible for initiating human skin cancers.[5] The UV solar radiation that reaches the face of the Earth consists of 95% UV-A and 5% UV-B components. Solar irradiation is known to produce different types of DNA lesions such as cyclobutane pyrimidine dimers, pyrimidine–pyrimidine (6–4 lesions) photoproducts, and thymine glycols. Whereas UV-B radiation mostly produces pyrimidine dimers by direct action, which can result in alpha–helical conformational changes. UV-A radiation can generate oxidative DNA damage indirectly by the generation of reactive oxygen species.[6] Current methods applied to investigate DNA damage mainly involve extraction, isolation and purification of the DNA prior to performing single cell gel electrophoresis or AFM. A rapid and direct alternative to such complex procedures is FTIR spectroscopy, in particular, synchrotron FTIR with the advantage that changes in nuclear DNA resulting from UVR exposure can be examined *in situ* while the cells are still functional. To the best of our knowledge there have been only a few other FTIR studies which have investigated cellular damage in response to UV-B irradiation. [7-9] In the studies by *Pozzi et al.* and Giambattista *et al.* [7,8] only UV-B was investigated that does not mimic sunlight directly, which is important aspect of this study. Moreover, in these studies a population of cells was investigated with Attenuated Total Reflectance (ATR) and hence the intra-population variability of UVR irradiation responses at the single cell level could not be determined as was achieved in this study. Furthermore, irradiation of isolated nuclei enabled the investigation of the protective capacity of the cell against DNA damage in the nucleus. The ATR–FTIR system used by Giambattista *et al.* and Pozzi *et al.* had a depth of penetration of 2–3 μm, which would not enable the interrogation of the entire nucleus given a typical cell has a thickness of ~5-10 μm and hence one would access only part of the nucleus at best, with the resultant spectrum mainly comprised of information from membrane and cytosol components. Nevertheless, they did report spectroscopic changes attributed to changes in the alpha–helical structure, which they deduced were from histone proteins within the nucleus.

Ali *et al.* applied Raman spectroscopic mapping coupled with statistical analysis to study skin damage caused by solar radiation in a human skin model. The model employed in that study consisted of keratinocytes and dermal fibroblasts exposed to 200–800 kJ/m^2 of UVR using an Oriel solar simulator as the radiation source. The K–means cluster analysis of Raman spectral maps indicated that morphological differences between various types of

cells resulted in the separate clustering of spectra from irradiated cells and controls not exposed to radiation, with an absence of DNA peaks reported in spectra acquired from irradiated samples. The researchers concluded that both DNA damage and changes in lipidic content were a consequence of the UVR exposure.[9] This previous work was able to resolve UVR-induced changes at the tissue level using Raman spectroscopy. In this study we extend this approach by attempting to resolve changes in sub-cellular structures within individual cells. In addition, we employ a multimodal investigative approach combining Raman and synchrotron IR microspectroscopies to study UVR induced changes in biological cells.

Specifically, UVR-induced DNA damage was studied *in situ* using cells from human skin melanoma COLO 679 cell line and extracted nuclei with a combination of synchrotron FTIR (SR-FTIR)and Raman microspectroscopy. The complementary nature of the infrared and Raman measurements provided a much more comprehensive and corroborative information about UVR induced DNA changes than has been reported previously.

Experimental

Cells and nuclei

Human skin melanoma cells from the COLO 679 cell line (ATCC PCS–200–013) were prepared as follows. Cells were cultured in RPMI 1640 supplemented with 2 mM glutamine and 10% of Foetal Bovine Serum (FBS) as previously reported[10].

Cellular nuclei were extracted for comparison after cells had been incubated for 24 h and 48 h, post-irradiation, following the procedure described by Junaid *et al.*[11] Cells were trypsinised, centrifuged (4 min, 1400 r.p.m) and then suspended in ice–cold nuclear extraction buffer [320 mM sucrose, 5 mM $MgCl_2$, 10 mM HEPES, and 1% Triton X–100 (pH 7.4)]. The suspension was vortexed gently for 10 s and incubated on ice for 10 min. Nuclei were collected by centrifugation at 2000 g and washed twice with nuclear wash buffer [320 mM sucrose, 5 mM $MgCl_2$ and 10 mM HEPES (pH 7.4)]. Freshly isolated nuclei were suspended in saline solution for the measurements.

Ultraviolet radiation exposure

Two types of substrates were utilised for the spectroscopic measurements: a) calcium fluoride windows (1 mm thickness and 10 mm in diameter) for FTIR studies on the living cells and isolated nuclei, b) aluminium coated Petri dishes (35 mm in diameter) for Raman measurements.

Cells were seeded onto substrates 24 hours prior to treatment (1.5 x 10^4 cells per one calcium fluoride window). Melanocytes were irradiated as a monolayer so that each cell was exposed equally. Before radiation exposure the majority of culture medium was removed, leaving ~300 µL of medium to prevent drying. Three different irradiation times were applied: 24 sec, 4 mins and 40 mins.

UV radiation (UVR) was provided by a single Q–Panel fluorescent tube (UV-A–340, Q–PANEL CO. USA). Cellulose triacetate sheet (100 µm thick Kodacel; Kodak-Eastman, NY, USA) was applied to the front of the lamp assembly to act as a filter preventing any UV-C radiation (wavelengths <280 nm) from reaching the samples, because this type of UV radiation is not a component of sunlight reaching the Earth's surface. The tubes were installed in a batten luminare positioned directly in front of the Petri dishes containing the cell samples. The distance between radiation sources and the samples was 1.5 cm with the power density of UV-B and UV-A radiation measured at ~2.44 W/m^2 and ~2.96 W/m^2 (unweighted), respectively,using a spectroradiometer system comprising an Acton Research Corporation (Massachusetts, USA) Model 300i, 300 mm focal length monochromator, an Acton Research Corporation model PD-439 photomultiplier tube detector, with light brought to the monochromator via a 3 metre fibre optic incorporating a quartz glass diffuser element (Acton Research Corporation). Data were acquired using an Acton Research Corporation NCL model data acquisition module and SpectraSense software, with the spectroradiometer calibrated against a 1000 W tungsten–halogen standard lamp (Oriel Corporation, Connecticut, USA), traceable to the National Institute of Standards, USA. Wavelength calibration was achieved using emission lines from a mercury lamp.

UV-A and UV-B radiation dosages were weighted using the internationally recognised erythema reference action spectrum[12] calculated for the applied irradiation times: 24 seconds (UV-A 78 J/m^2, UV-B 72 J/m^2), 4 minutes (UV-A 787 J/m^2, UV-B 718 J/m^2), and 40 minutes (UV-A 7872 J/m^2, UV-B 7180 J/m^2). The irradiation regimes were chosen such that weighted UVR doses were comparable with the minimum doses of UVR causing redness of Caucasian (295 J/m^2), Asian (200 J/m^2) and Afro–American (765 J/m^2) skin types[13]

After irradiation, 2 ml of culture medium was added to each dish and the cells were incubated for 24 and 48 hours. Cellular nuclei were extracted from the cells after incubation time of 24 and 48 h.

SR–FTIR and Raman measurements

Approximately 80 single cells/nuclei from each group of cells treated with one dose of UVR and incubated for either 24 or 48 h incubation time were measured. Three independent experiments were conducted. SR-FTIR measurements were performed on the FTIR microspectroscopy beamline (2BM1B) at the Australian Synchrotron. The beamline is equipped with a Bruker V80v FTIR and Hyperion microscope, with narrow band MCT detector. Spectra were recorded in transmission mode with a spectral resolution of 4 cm^{-1} in the spectral range 4000 cm^{-1} – 750 cm^{-1} with 64 interferograms co-added.

Cells were also investigated with Raman microspectroscopy. A WiTec alpha300 R confocal Raman Microscope equipped with Nd–Yag 532 nm laser and a 60× water immersion objective was used for measurements of cells and nuclei.

Two– and three–dimensional Raman maps were recorded using the same instrument, with the spatial resolution estimated to be ~d=λ/2 (~270 nm). The step–size for the Raman mapping was 0.25 µm in the sample plane (*xy* direction) and 0.8 µm in *z* direction. The laser exposure time was set to 2 sec with the laser power at the sample ~15 mW. Each single channel spectrum was acquired with a resolution of 2 cm^{-1} in the spectral range 4000 cm^{-1} – 200 cm^{-1}.

All Raman and IR spectra were processed in Opus 6.5 software (Bruker Optics) which included smoothing (number of

smoothing points: 13) and baseline correction (rubber–band correction algorithm; 16 baseline points; with 2–3 iterations).

Results and Discussion

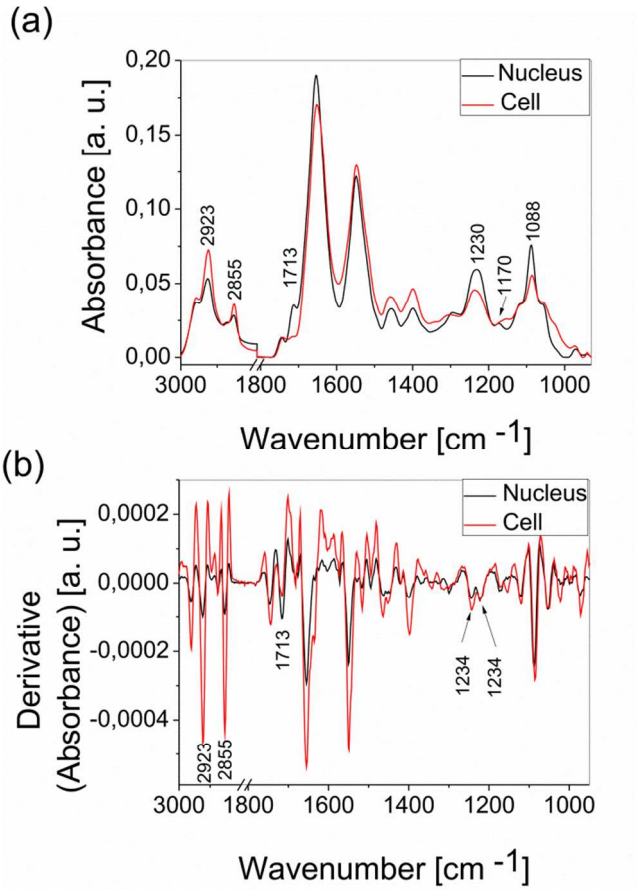

Fig. 1 Mean spectra collected from single control COLO–679 cells and single isolated cell (COLO–679) nuclei (a) along with the mean second derivatives for those spectra (b).

A comparison of 80 mean SR-FTIR spectra and their corresponding second derivatives of the control cell and isolated cellular nuclei are presented in Fig. 1. Nuclei are less complex in terms of composition compared to whole cells, and consequently the DNA bands appear more pronounced in nuclei spectra. The major DNA bands observed in nuclei include the O–P–O stretching modes at 1088 cm^{-1}, 1170 cm^{-1}, 1230 cm^{-1} and C–O stretching at 970 cm^{-1} as well as the base stacking mode (C=O stretching in purines and pyrimidines rings at 1713 cm^{-1}).[14]

Dose dependent response to UV radiation studied by SR–FTIR in isolated cellular nuclei after 24 hours post irradiation

The single isolated (24 hours post irradiation) cellular nuclei spectra and their second derivatives are presented in Fig. 2. UV dose dependent spectral changes are observed and include a decrease in intensity of the C=O stretching mode at 1713 cm^{-1} caused by base–pair damage such as purine and pyrimidine dimer formation along with 6–4 lesions. We observed also a shift of the O–P–O asymmetric stretching band from 1230 cm^{-1} to 1240 cm^{-1}, which has been associated with conformation change previously observed for the B–DNA to A–DNA transition detected in cells and isolated nuclei in response to dehydration.[14,15] DNA conformational changes could play an important role in the resistance to DNA damage.[17] Another important observation is an intensity increase in the Amide II band at 1549 cm^{-1} possibly related to an increase in transcriptional processes in response to DNA repair. An intensity decrease in the $\nu_{symm}(PO_2^-)$ and $\nu_{asymm}(PO_2^-)$ at 1088 cm^{-1} and 1230 cm^{-1} – 1240 cm^{-1}) is observed for cells irradiated for 4 minutes and 40 minutes. It is hypothesised that after exposure the cells are halted in the G1 phase during DNA repair. It has previously been shown that cells in the G phase have smaller phosphodiester bands [15,16] because during the repair process DNA cannot be replicated leading to lower DNA content.

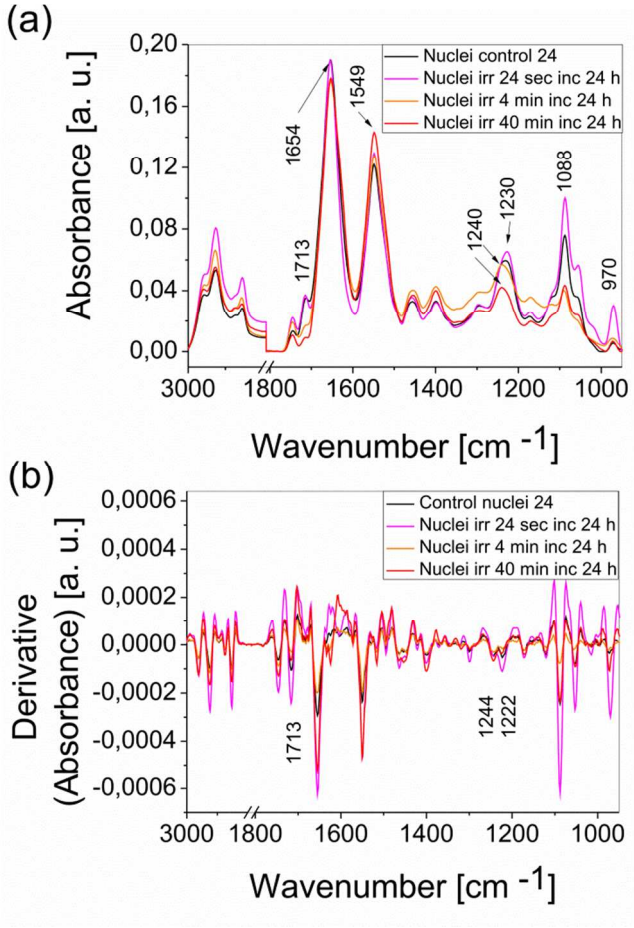

Fig. 2 The averaged spectra collected from single isolated COLO–679 cellular nuclei, control and irradiated with 3 various UV doses, then incubated for 24 hours along with the averaged second derivatives for those spectra.

PCA was applied to the second derivatives of nuclei spectra in the spectral range from 1800 cm^{-1} to 1030 cm^{-1}. PCA was performed in Unscrambler (Camo, Norway) software using the NIPALS algorithm. Cross validation was applied as a validation method and the data mean-centered. In this PCA model the DNA backbone bands were investigated together with bands from the protein modes. Four clusters for the four groups of spectra are well delineated on the PC–1 vs. PC–2 Scores Plot (Fig. 3a). PC–1 explained 63 % of total variance and it is positively correlated with the $\nu_{asymm}(PO_2^-)$ at 1222 cm^{-1} (characteristic for B-DNA in control nuclei) and negatively correlated with the $\nu_{asymm}(PO_2^-)$ at 1244 cm^{-1} (typical for A-DNA isolated from the nuclei of irradiated cells). PC–2 explained 11% of total variance and was positively correlated to the $\nu_{asymm}(PO_2^-)$ at 1244 cm^{-1} for cells irradiated for 40 min and also half of the amount of cells irradiated for 4 mins. PC-2 is positively correlated to the base-stacking mode at 1714 cm^{-1} consistent with DNA conformational changes in cells irradiated for 40 mins and to some extent with cells irradiated for 4 mins. The Loadings Plot confirms that variation in the intensity and positions of phosphodiester bands, together with the base stacking mode band (~1714 cm^{-1}) and the intensity of Amide II band (~ 1545 cm^{-1}) is responsible for general clustering observed in the Scores Plot.

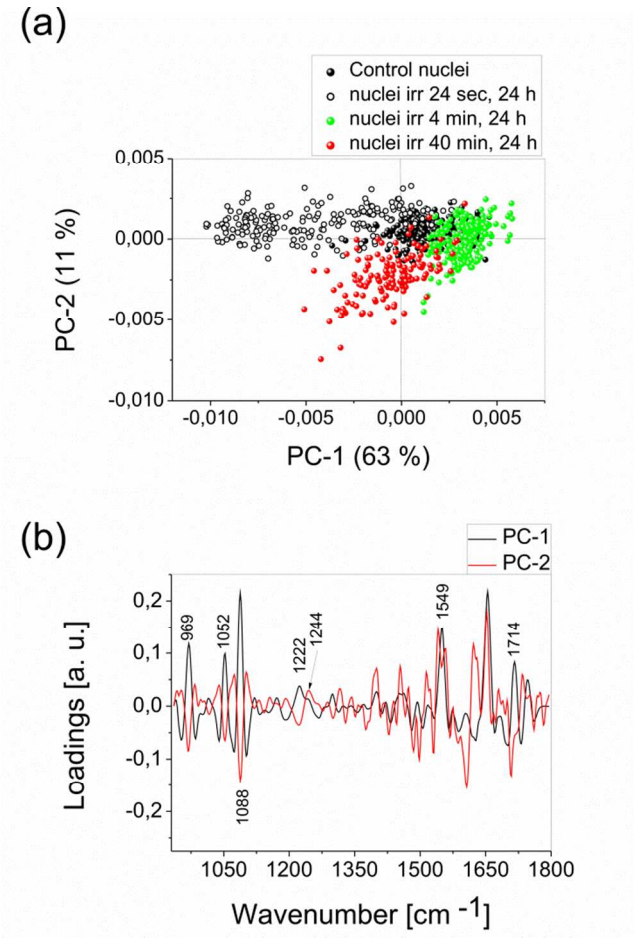

Fig. 3 The results of PCA analysis showing a PC–1 vs. PC–2 two–dimensional Scores Plot (a) with the corresponding Loadings Plot for PC–1 and PC–2 (b) applied to 4 groups (nuclei isolated from control and irradiated with three different doses of protons and incubated for 24 hours cells) of second derivative spectra in spectral range 1030 cm^{-1} – 1800 cm^{-1}.

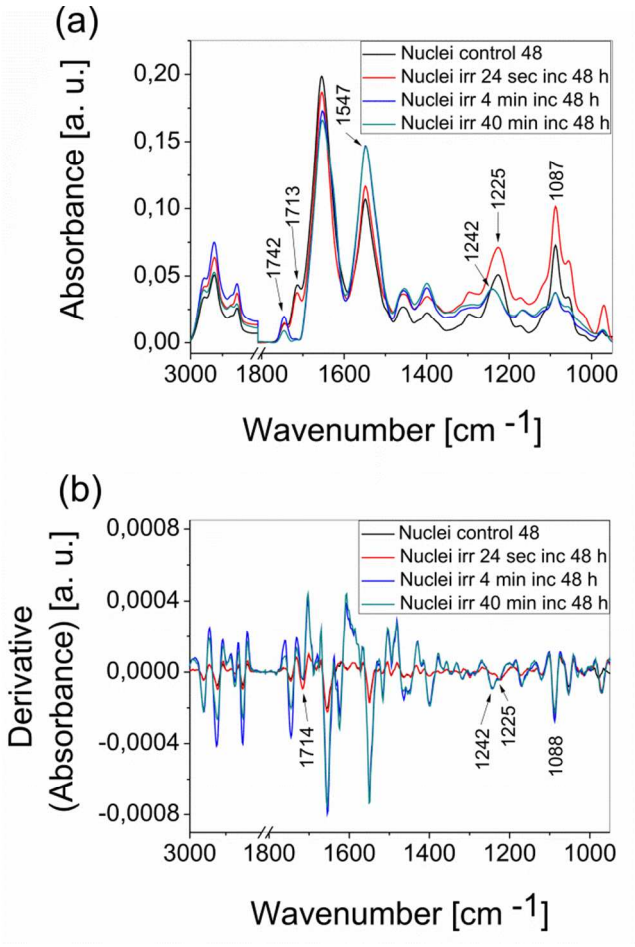

Fig. 4 The averaged spectra collected from single isolated COLO–679 cellular nuclei, including control and irradiated with 3 different UV doses, then incubated for 48 hours (a) and the averaged second derivative of those spectra (b).

Dose dependent response to UV radiation studied by SR–FTIR in isolated cellular nuclei after 48 hours post irradiation

The FTIR spectra from single isolated (48 hours post–irradiation) cellular nuclei and their second derivatives are presented in Fig. 4. Forty–eight hours after irradiation the UVR dose dependent spectral changes are similar to those observed 24 hours post irradiation as described above. PCA was applied to the second derivative nuclei spectra in the spectral range from 1800 cm^{-1} to 1030 cm^{-1}. Fig. 5 shows that the spectra of nuclei isolated from control and irradiated for 24 seconds with UVR are clustered together in the PC–1 versus PC–2 Scores Plot. This suggests that cells irradiated for 24 seconds had already repaired the DNA damage after 24 hours of incubation. There is no well defined boundary between clusters of spectra of nuclei isolated from cells irradiated for 4 minutes and 40 minutes.

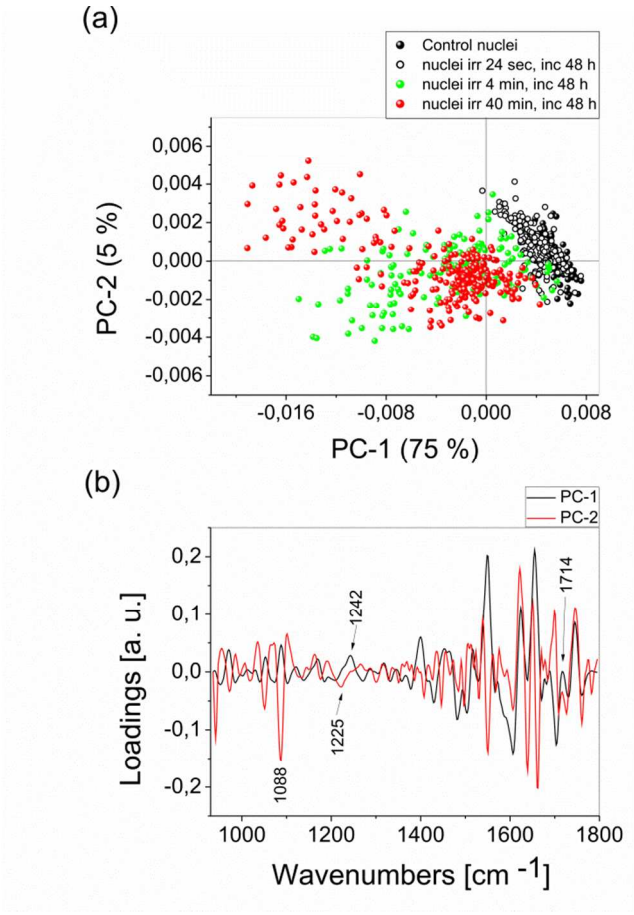

Fig. 5 The results of PCA analysis applied to 4 groups of second derivative spectra (nuclei isolated from control and irradiated with three various doses of protons and incubated for 48 hours cells) in spectral range 1800 cm^{-1} – 1030 cm^{-1} showing a three–dimensional Scores Plot (a) along with the corresponding Loadings Plot (b).

This suggests that the cellular responses including DNA repair and protein composition are similar in the two groups of cells. The general separation of spectral clusters occurred along PC–1, which explains 75% of total variance. PC–1 is positively correlated with the band at 1224 cm^{-1}, characteristic for control nuclei and nuclei isolated from cells irradiated for 24 seconds and negatively correlated with the band at 1244 cm^{-1}, characteristic for nuclei isolated from cells irradiated by UV for 4 and 40 minutes. Both loadings are positively correlated to the C=O stretching mode of lipids (~1745 cm^{-1}), which indicated that lipid changes are also involved in the DNA repair process. To confirm this hypothesis PCA was applied to the major lipid bands in the CH_2, CH_3 stretching region on spectra collected from nuclei isolated from control and irradiated cells. The results are presented in Fig 6, which shows a Scores Plot (Fig. 6a) exhibiting a clear separation between control and irradiated nuclei in this spectral region. The clustering indicates that lipids are involved in the cellular response to UVR as evidenced by the Loadings Plot (Fig. 6 b), which shows that the symmetric and antisymmetric stretching modes of methyl and methylene groups are responsible for the clustering.

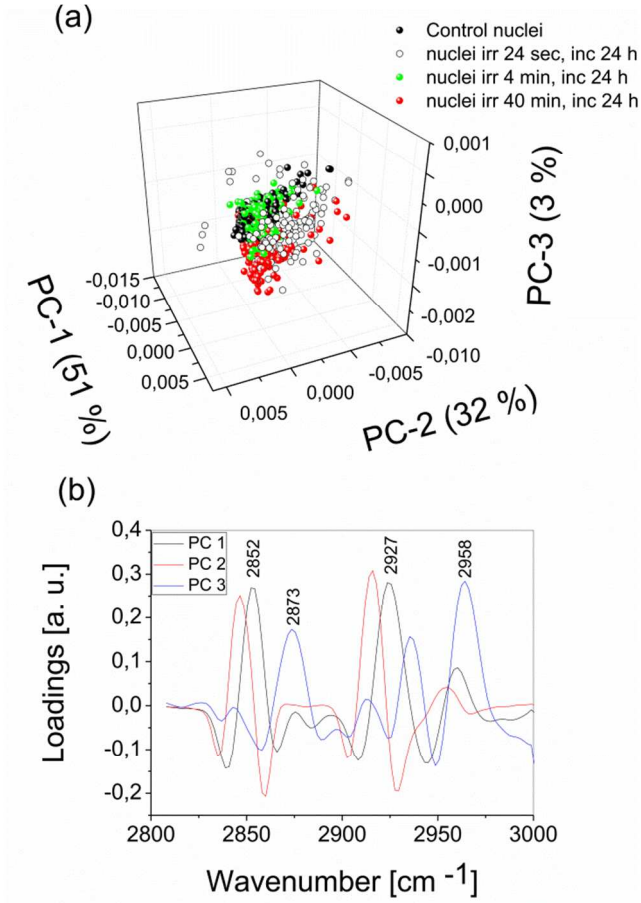

Fig. 6 The results of PCA analysis applied to 4 groups of second derivative spectra (nuclei isolated from control and irradiated with three various doses of protons and incubated for 24 hours cells) in spectral range 3000 cm^{-1} – 2800 cm^{-1} showing a three–dimensional Scores Plot (a) along with the corresponding Loadings Plot (b).

Dose dependent response to UV radiation in living cells studied using SR–FTIR

The averaged spectra from living cells including the control and those irradiated by UVR prior to incubation for 24 hours and 48 hours are presented in Fig. 7a and Fig. 7b respectively.

Dose dependent changes were not as easily identified in single cell spectra compared with single cellular nuclei spectra. It may be that the detection of an unambiguous UVR influence is difficult because of the complex cellular structure. This is not the case in isolated nuclei because there are fewer absorbing macromolecules and the DNA bands are more pronounced compared to those in the spectra of the whole cells. The data from samples incubated for 24 hours after irradiation indicates a shift of O–P–O asymmetric stretching band from 1232 cm^{-1} to 1236 cm^{-1} and for cells incubated for 48 hours from 1236 cm^{-1} to 1242 cm^{-1} which is likely associated with a partial conformational

change from B–like DNA to an A–like DNA conformational state similar to the one observed when cells and nuclei are dehydrated [14,17].

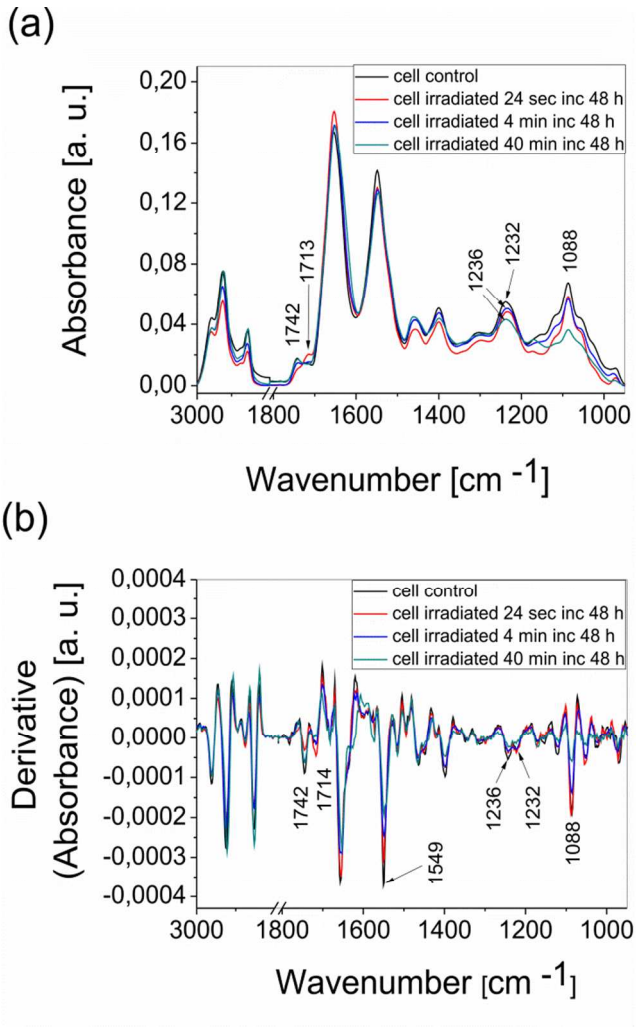

Fig. 7 The averaged spectra collected from single COLO–679 cells, including control and irradiated with 3 different UV doses, then incubated for 48 hours (a) and the corresponding second derivatives of those averaged spectra (b).

The intensity decrease in the phosphate bands in cells irradiated for 4 minutes and 40 minutes is consistent with the view that at 48 hours post–irradiation the cells were in the G1 phase repairing their DNA.

A few PCA models were applied to the spectra and their second derivatives from cells to investigate relationships within the data (data not shown). The results showed some clustering but the boundaries were not well defined.

Post irradiation recovery time dependent response to UV radiation studied by SR–FTIR in isolated cellular nuclei and in living cells

Time dependent differences in second derivative spectra of isolated nuclei from irradiated and control cells along with living cells irradiated with UVR and then incubated for 24 and 48 hours were investigated with PCA. The results are presented in Fig. 8 for each dose separately.

On each Scores Plot for the isolated nuclei spectra, 3 clusters are observed: 1) the spectra of control nuclei isolated after 24 hours of incubation and control nuclei isolated after 48 hours of incubation are clustered together, 2) two other clusters associated with the nuclei isolated from irradiated cells and incubated for 24 hours and 48 hours, respectively. Both controls i.e. 24 and 48 hours are clustered together, which demonstrates that the actual incubation time has no effect on the observed clustering for the irradiated samples.

The Loadings Plots indicate that the same bands are responsible for the spectral separation as described earlier ("Dose dependent response to UV radiation studied by SR–FTIR in isolated cellular nuclei" section above) for nuclei and cellular spectra.

Raman microspectroscopy

The variability of Raman single-point spectra collected from single cells using a 60× water immersion objective did not allow for dose dependent damage detection. We hypothesise that fine scale spatial variability in cellular composition may, at least partially, be responsible for this. The laser beam spot is very small in comparison to a cell, a nucleus and other organelles, hence the differences in chemical structure of cellular components could result in a high degree of spectral variability at different spatial locations.

PCA was applied to the spectra and their second derivatives to investigate any general clustering in the data. However, PCA did not show any distinct clusters when using second derivative spectra from control cells and cells irradiated with different doses of UVR perhaps because of the confounding effect of the spectral variability at different spatial locations described above.

Raman imaging

Raman 3D imaging was applied to achieve a more complete picture of the effects of UVR on single cells and nuclei. In Fig. 9 the integrated area under the O–P–O asymmetric stretching peak (1255 cm^{-1} – 1225 cm^{-1}) normalised to Amide I band (1680 cm^{-1} - 1600 cm^{-1}) of nucleic acids is shown for isolated cellular nuclei from control (Fig. 9a) and irradiated by UVR for 4 mins and then incubated for 48 hours (Fig. 9b). The distribution of this band was homogeneous for the control sample and inhomogeneous for irradiated cellular nuclei. This visible heterogeneity may indicate chromatin condensation, which is characteristic of late apoptosis.

The 3D image for the integrated area under CH_2 – CH_3 stretching region (2900 cm^{-1} – 2650 cm^{-1}) normalised to Amide I band (1680 cm^{-1} -1600 cm^{-1}) for an isolated cellular nucleus from a cell irradiated with UVR for 40 minutes and then incubated for 24 hours is presented in Fig. 10. Collecting 3D cell/cellular nuclei maps provides full molecular information about the sample with a

spatial resolution approaching the diffraction limit. The inhomogeneous distribution of the integrated area under the CH_2, CH_3 stretching region indicated lipid deposits in the nucleus after exposure to UVR.

To observe the distribution of functional groups characteristic of the biomolecules in isolated cellular nuclei Unsupervised Hierarchical Cluster Analysis (UHCA) was applied. Some typical results are presented in Fig. 11.

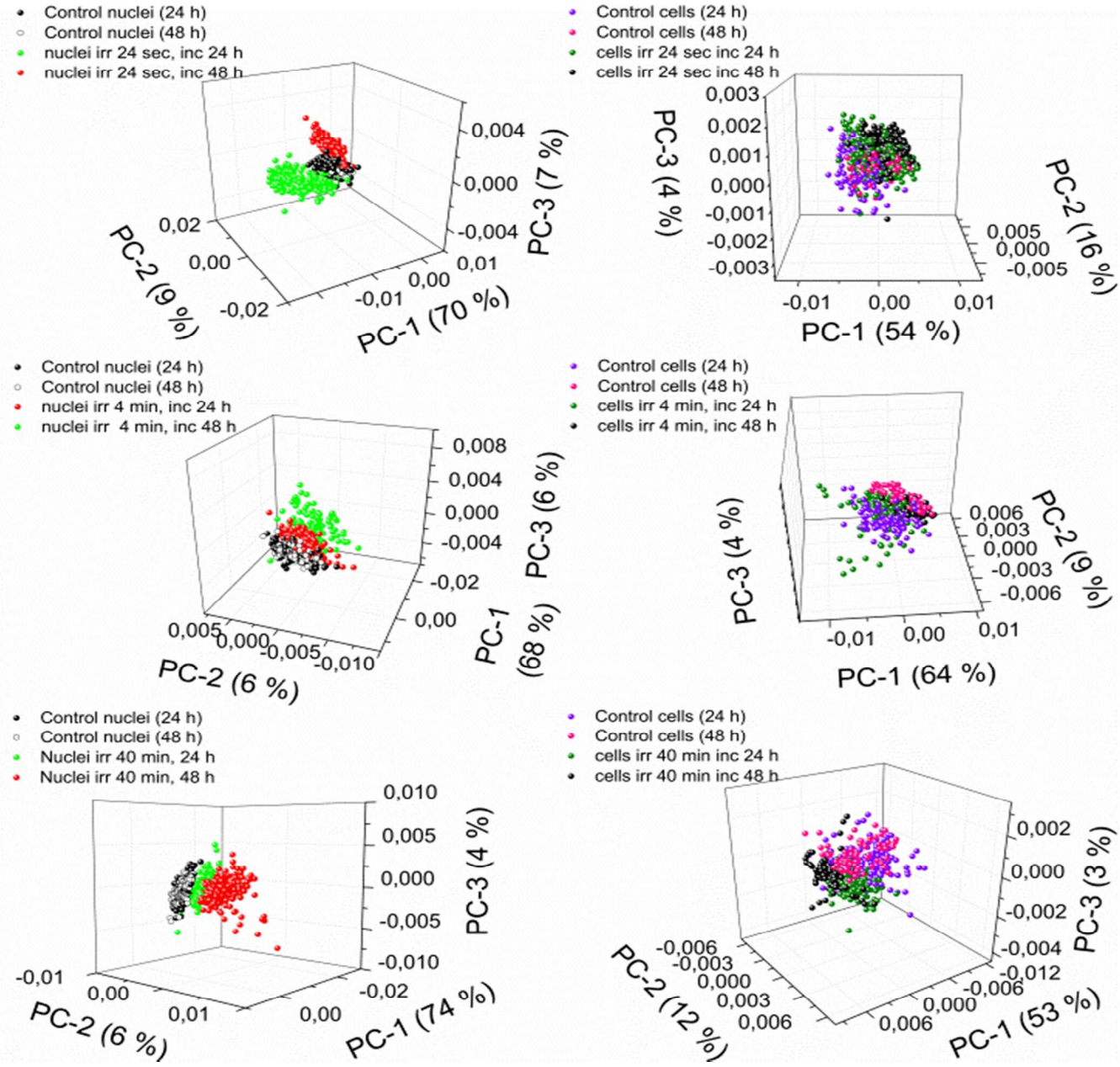

Fig. 8 A comparison of PCA results, which was applied to 4 groups of second derivative spectra (nuclei isolated from control and irradiated cells and then incubated for 24 and 48 hours and living cells treated in the same way) for each dose separately in spectral range 1800 cm^{-1} – 1030 cm^{-1} showing a three–dimensional Scores Plots of nuclei and cell spectra separated

Cite this: DOI: 10.1039/c0xx00000x

www.rsc.org/xxxxxx

ARTICLE TYPE

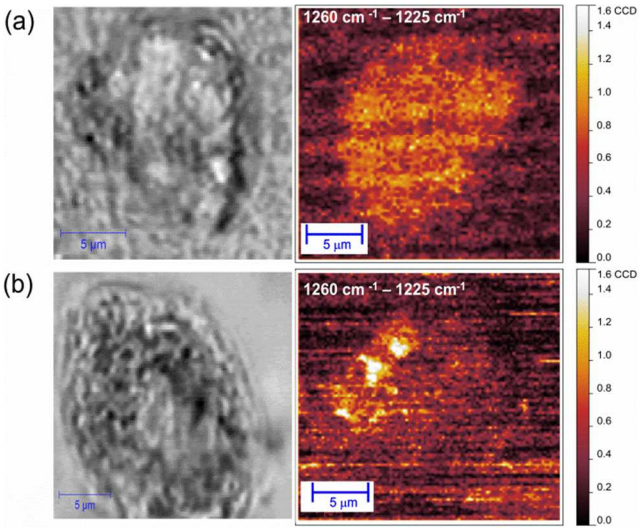

Fig. 9 The integrated area under the O–P–O asymmetric stretching peak (1260 cm^{-1} – 1225 cm^{-1}) normalised to Amide I peak (1680 cm $^{-1}$ -1600 cm^{-1}) for isolated control cellular nucleus (a) and nucleus isolated from cell irradiated with UVR for 4 minutes and then incubated for 48 hours (b).

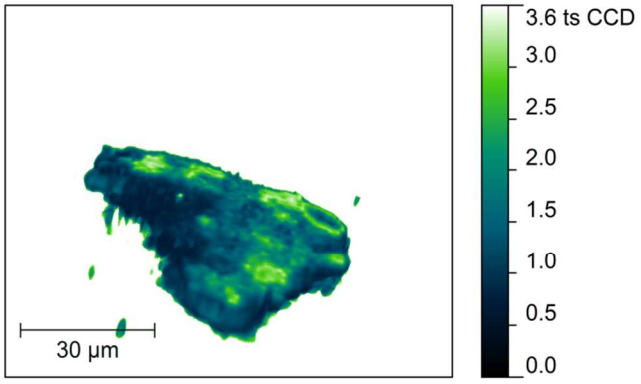

Fig. 10 The distribution of integrated area under CH_2 CH_3 stretching region (2900cm^{-1} – 2650 cm^{-1}) normalised to Amide I peak (1680 cm $^{-1}$ - 1600 cm^{-1}) for isolated cellular nuclei from cell irradiated with UVR for 40 minutes and then incubated for 24 hours.

The nuclei isolated from control cells (Fig. 11 a) were divided into two distinct clusters (blue and brown). The averaged spectra from blue and brown areas are presented on the same figure. There are two main differences between the spectra. In only the spectrum colour-coded brown a band at 838 cm^{-1} is observed, which is assigned to C–O, and C–P–O stretching modes in the nucleic acid backbone and additionally the $\nu_{asymm}(PO_2^-)$ is slightly shifted from 1257 cm^{-1} to 1251 cm^{-1} in the blue coded spectrum. These changes are consistent with a B–like DNA to an A–like DNA conformational change [18,19] or the result of a different DNA/RNA ratio.[20,21] Comparison of the mean spectra indicates that in the brown coded region of the sample there is possibly more RNA than in the blue coded region.

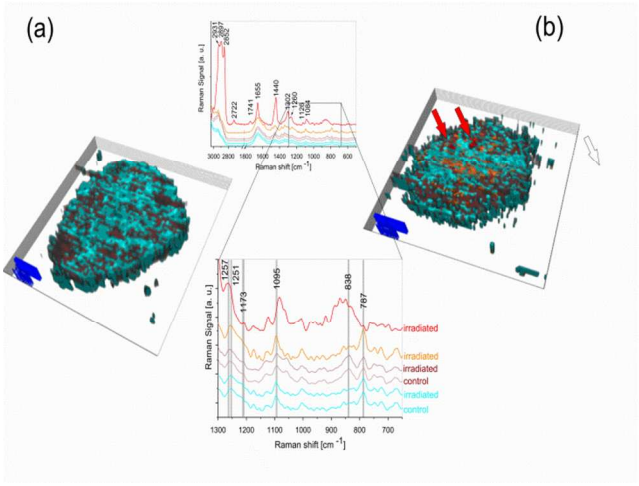

Fig. 11 The UHCA map of nuclei isolated from a control cell (a) and irradiated for 4 minutes then incubated for 48 hours (b) cell. The voxels and the averaged spectra from each area are marked by the same colours. The lipid accumulations are marked by arrows.

Very similar spectra were detected in the 3D Raman maps of nuclei, which were isolated from irradiated cells. The spectra and the related voxels are marked by the same colours as in Fig. 11a and Fig 11 b. Two additional clusters (orange and red) were identified in the irradiated cells. The orange coded clusters in fig 11 indicate regions of high concentration of nucleic acids possibly associated with regions of chromatin condensation. The averaged spectrum from the red coded clusters (observed in all layers of damaged nuclei, marked by arrows in Fig. 11 b) showed these clusters were associated with lipids. The strong signals from lipids and fatty acids were corroborated by observation of spectral intensity differences such as the stretching motions of methyl and methylene groups in the spectral range 3050 cm^{-1} – 2800 cm^{-1}, the ν(C=O) from lipids at 1741 cm^{-1}, ν(C=O) of the carbonyl group at 1655 cm^{-1}, δ(CH_2) at 1440 cm^{-1}, $\delta_t(CH_2)$, $\delta_w(CH_2)$ at 1302 cm^{-1} highlighted in Fig. 11 (red coded spectrum).

The intra–nuclear lipid deposits in isolated nuclei of control COLO 679 cells were below the Raman microspectroscopic spatial resolution detection limit if they are indeed present. However, in intact cells, phospholipids associated with chromatin appeared to be localised around the decondensed chromatin and near newly synthesised RNA.[22] The most common nuclear lipid is sphingomyelin, followed by phosphatidylethanolamine, phosphatidylserine, phosphatidylinositol, phosphati-dylcholine, plasmalogens and cholesterol[22]. Many enzymes such as sphingomyelinase, sphingomyelin-synthase, reverse sphingomyelin-synthase and phosphatidylcholine-dependent phospholipase C have been found in cellular nuclei and previously described.[22] An increase of sphingomyelin synthase activity and diacylglycerol has been

associated with chromatin condensation and has been reported for apoptotic cells.[23] Albi *et al.* studied intra-nuclear lipid metabolism in relation to the apoptosis induced by UV radiation. The activation of phosphatidylcholine and sphingomyelin metabolism indicates accumulation of those lipids during apoptosis.[24] Wang *et al.* reported that damaging factors like perfluorooctanoic acid (PFOA) result in lipid droplet accumulation in the nucleus of hepatic cells and correlated this with chromatin condensation in response to apoptosis.[25]

Shulze *et al.* mapped mammalian cellular nuclei in ethanol fixed cells by Raman microspectroscopy. The data was analyzed using PCA but there was no mention of intra-nuclear lipid deposition.[21] Isolated cellular nuclei (fixed in paraformaldehyde) were also studied using Raman scattering by Pijanka *et al* who like Shulze et al. did not report any accumulation of intra-nuclear lipids.[26] Pliss *et al.* applied Coherent anti-Stokes Raman Scattering (CARS), which enabled the detection of intra-nuclear lipids even in low concentrations as found in centromeric heterochromatin (~14 mg/mL) and/or the nuclear speckles (~10 mg/mL).[27] In the present study lipid accumulation was detected in nuclei damaged by UVR and isolated from irradiated cells. These lipids are probably associated with an increase in lipid metabolism during apoptosis[24] or lipid droplet accumulation[25] associated with the formation of apoptotic bodies.

From another point of view lipid biosynthesis plays an important role in cancer cell migration and invasion, and also in the induction of tumor angiogenesis. These processes are considered to be crucial for the dissemination of tumor cells and formation of metastases, which constitute the main cause of cancer mortality.[28, 29] These results are in agreement with the increasing body of evidence that lipid accumulation is a hallmark of aggressive cancer cells, and is involved in the production of membranes for rapid cell proliferation. [30]

Our data allowed for the detection of particular types of lipids. Spectra collected from the places where lipid accumulation was detected (Fig. 10 red spectrum) is indicative of cholesterol (C–H bending at 2933 cm^{-1}, CH_2 scissoring deformations at 1440 cm^{-1}),[30, 31] cholesteryl ester (C=O bond of the ester linkage at 1741 cm^{-1}, CH_2 scissoring deformations at 1440 cm^{-1} and CH stretching at 2897 cm^{-1} and at 2852 cm^{-1}).[30, 31] The appearance of the C=C stretching at 1655 cm^{-1} [32] indicates unsaturated fatty acids are also constituents of these lipid droplets. Sterols, mainly cholesterol and cholesteryl-esters which modulate the fluidity of the lipid bilayer [29], are important for membrane function, which is in good agreement with our hypothesis that observed lipid accumulation in COLO-676 cells might be related to cellular preparation prior to intensive proliferation. A number of chemical inhibitors of lipid biosynthesis, most prominently inhibitors of fatty acid synthase, have been already investigated and it seems that they will play an important role in metastases prevention.[29] Therefore high resolution spectroscopic and 3-dimensional Raman imaging are very useful tools to detect and understand the lipid processes that can potentially lead to metastasis.

Conclusions

In this study the response of the melanoma cell line COLO–679 to environmentally-relevant doses of UVR exposure was investigated using SR–FTIR and Raman microspectroscopy in combination with multivariate data analysis. Clear spectral changes were observed associated with biochemical processes caused by the radiation exposure.

Using SR-FTIR we have demonstrated a dose dependent intensity decrease of the C=O stretching mode, which we hypothesise is the result of base–pair damage such as purine and pyrimidine dimer formation or 6–4 lesions. A shift in the $\nu_{asymm}(PO_2^-)$ indicates a partial conformation change from B–like DNA to an A–like DNA conformation. Additionally, an intensity increase in the Amide II band was observed following UV radiation exposure possibly related to an increase in DNA repair and hence protein content. The observed intensity decrease of O–P–O symmetric and asymmetric stretching for cells irradiated for 4 minutes and 40 minutes, was identified as a spectroscopic marker for cells stopped in G1 phase after radiation exposure and during the DNA repair stage. Nuclei isolated after cell irradiation exposure showed the most dramatic changes in response to radiation using SR–FTIR. The spectral profiles of isolated nuclei and living cells are similar in appearance, except in the nuclei spectra the DNA bands are more clearly defined. High variability of Raman single-point spectra collected from random locations on single cells or nuclei made the observation of cellular response to UV radiation very difficult to define unequivocally. To achieve a more complete picture of the effects of UV radiation on cells or cellular nuclei multidimensional Raman mapping was successfully applied. We report for the first time that Raman mapping of cellular nuclei isolated 48 hours after radiation exposure shows inhomogeneous distribution of phosphodiester band intensity and bands associated with intra-nuclear lipid deposition. SR-FTIR / Raman results that associate apoptosis to an upregulation of lipid intensity should be compared with well-validated biochemical assays of apoptosis for melanoma cells undergoing the same experimental conditions. An application of combined staining of the cells with Annexin V FITC and Propidium Iodide (PI) allowing for early apoptosis (Annexin V FITC positive and PI negative cells), late apoptosis (Annexin V FITC positive and PI positive cells) and necrosis (Annexin V FITC negative and PI positive cells) recognition in single cells[34] is recommended.

These results indicate chromatin condensation and the possible formation of apoptotic bodies, which are characteristic for the late apoptotic process associated with UV radiation exposure. The application of a multimodal approach for UVR studies on living single cells and isolated nuclei provided a basis for understanding the macromolecular changes that may underpin skin cancer.

Notes and references

[a] *The Henryk Niewodniczanski Institute of Nuclear Physics, PAN, 31-342 Kraków, Poland. Fax: +48 01 2662 8458; Tel: +48 01 2662 8200; E-mail: dyrektor@ifj.edu.pl*

[b] *Centre for Biospectroscopy, School of Chemistry, Monash University, 3800, Victoria, Melbourne, Australia. Fax: +61 3 9905 4597; Tel: +61 3 9905 4593; E-mail: bayden.wood@monash.edu*

[c] *Australian Synchrotron, 800 Blackburn Rd Clayton, Victoria 3168, Melbourne, Australia. Fax: +61 3 8540 4200; Tel: +61 3 8540 4100; E-mail: info@synchrotron.org.au*

[d] *Department of Anatomy and Developmental Biology, Monash University, Wellington Road, Clayton, Victoria, 3800, Melbourne, Australia. Fax: +61 03 9902 9223; Tel: +61 03 9902 9100; E-mail: Anatomy@monash.edu*

[e] *BAM Federal Institute for Materials Research and Testing, Division 4.4 Thermochemical Residues Treatment and Resource Recovery, Unter den Eichen 87, D-12205 Berlin, Germany. Fax: +49 30 8112029; Tel: +49 30 81040; E-mail: info@bam.de*

1 World Health Organization. Ultraviolet radiation and the INTERSUN Programme – how common is skin cancer? http://www.who.int/uv/faq/skincancer/en/index1.html (accessed 2010 January 12)

2 M. P. Staples, M Elwood, R. C. Burton, J. L. Williams, R. Marks and G. G. Giles, *Med. J. Aust.,* 2006, **184**, 6;

3 http://www.cancer.org.au/about-cancer/types-of-cancer/skin-cancer.html (assessed in 2012)

4 J. K. Robinson, JAMA, 2005, **294**, 1541;

5 R. P. Sinha, and D. P. Hader, *Photochem. Photobiol. Sci.,* 2002, **1**, 225;

6 P. Moller, H. Wallin, and L. E. Knudsen, *Chem. Biol. Interact.,* 1996, **102**, 17;

7 D. Pozzi, P. Grimaldi, S. Gaudenzi, L. Di Giambattista, I. Silvestri, S. Morrone, and A. Congiu Castellano, *Radiat. Res.,* 2007, **168**, 698;

8 L. Giambattista, P. Grimaldi, S. Gaudenzi, D. Pozzi, M. Grandi, S. Morrone, I. Silvestri, and A. Congiu Castellano, *Eur. Biophys. J.,* 2010*,* **39,** 929;

9 S. M. Ali, F. Bonnier, K. Ptasinski, H. Lambkin, K. Flynn, F. M. Lyng and H. J. Byrne, *Analyst,* 2013*,* **138**, 3946;

10 E. Lipiec, G. Birarda, J. Kowalska, J. Lekki, L. Vaccari, A. Wiecheć, B. R. Wood, W. M. Kwiatek, *Radiat. Phys. Chem.,* 2013 **93** 135;

11 A. Junaid, M. C. Moon, G. E. J. Harding, and P. Zahradka, *Am. J. Physiol. Cell. Physiol.,* 2007*,* **292**, 919;

12 [CIE] Commission Internationale de l'Eclairage, Erythema reference action spectrum and standard erythema dose, CIE S007E-1998, CIE Central Bureau, Vienna, Austria, 1998;

13 F. Rouzauda, A. L. Kadekarob, Z. A. Abdel-Malekb, V. J. Hearinga, *Mutat Res.,* 2005 **571**, 133,

14 D. R. Whelan, K. R. Bambery, P. Heraud, M. Tobin, M. Diem, D. McNaughton and B. R. Wood, *Nucl. Acid Res.,* 2011*,* **39**, 5439;

15 D. R. Whelan, K. R. Bambery, L. Puskar, D. McNaughton, & B. R. Wood, *Analyst,* 2013, **138,** 3891;

16 K. S. Lee, D. Bumbaca, J. Kosman, P. Setlow and M . J. Jedrzejas, *Proc. Natl Acad. Sci.,* 2008, **105**, 2806;

17 H.-Y. N. Holman, R. Goth-Goldstein, E. A. Blakely, K. Bjornstad, M. C. Martin and W. R. McKinney, *SPIE,* 2000, **3918**, 57;

18 R. Marty, C. N. N'soukpoe–Kossi, D. Charbonnea, C. M, Weinert, L. Kreplak and H. A. Tajmir–Riahi, *Nucl. Acids Res.,* 2009, **37** 849;

19 Y. Guan, J. M. Benevides, Y. G. Gao, A. H. Wang, and G. J. Jr Thomas, *Nucl. Acids Res.,* 1998, **26**, 3892;

20 J. F. Neault, and H. A Tajmir–Riahi, *J. Biol. Chem*., 1997, **272**, 8901;

21 H. G. Schulze, S. O. Konorov, J. M. Piret, M. W. Bladesand and R. F. B. Turner, *Analyst.,* 2013, **138**, 3416;

22 E. Albi, and M. P. Viola Magni, *Biol. Cell.,* 2004, **96**, 657;

23 E. Albi, S. Pieroni, M. P. Viola Magni and C. Sartori, *J. Cell. Physiol*., 2003*,* **196**, 354;

24 E. Albi, S. Cataldi, G. Rossi, M. P. Viola Magni, M. Toller, S. Casani and G.Perrella, *Arch. Biochem. Biophys., 2008,* **478**, 52;

25 L. Wang, Y. Wang. Y. Liang, J. Li, Y. Liu, J. Zhang, A. Zhang. J. Fu and G. Jiang, *Scientific Reports.,* DOI: 10.1038/srep02174;

26 J. Pijanka, N. Stone, A. V. Rutter, N. Forsyth, G. D. Sockalingum, Y. Yanga and J. Sulé-Suso, *Analyst*, 2013, **138**, 2052;

27 A. Pliss, A. N. Kuzmin, A. V. Kachynski and P. N. Prasad, *Biophys. J*., 2010, **99**, 3483;

28 [28] C.J. Antalis, A. Uchida, K.K. Buhman, R.A. Siddiqui *Clin Exp Metastases,* 2011, **28,** 733;

29 F. Baenke, B. Peck, H. Miess, A. Schulze, *Dis Model Mech,* 2013, **6**, 1353;

30 K.M. Marzec, T.P. Wrobel, A. Rygula, E. Maslak, A. Jasztal, A. Fedorowicz, S. Chlopicki, M. Baranska*, J Biophotonics*, DOI: 10.1002/jbio.201400014;

31 A. Lattermann, C. Mattha¨us N. Bergner, C. Beleites, B.F. Romeike, C. Krafft, B.R. Brehm, J. Popp, *J Biophotonics*, 2013, **6**, 110;

32 P. Weinmann, M. Jouan, N. Q. Dao, B. Lacroix, C. Groiselle, J.-P. Bonte, and G. Luc, Atherosclerosis, 1998, **140**, 81;

33 C. Nieva, M. Marro, N. Santana-Codina, S. Rao, D. Petrov, A. Sierra, *PLoS ONE,* 2012, **7**, e46456;

34 A. Wnętrzak, E. Lipiec, K. Łątka, W. M. Kwiatek, P. Dynarowicz-Łątka *J. Mem. Biol*. DOI 10.1007/s00232-014-9674-8.

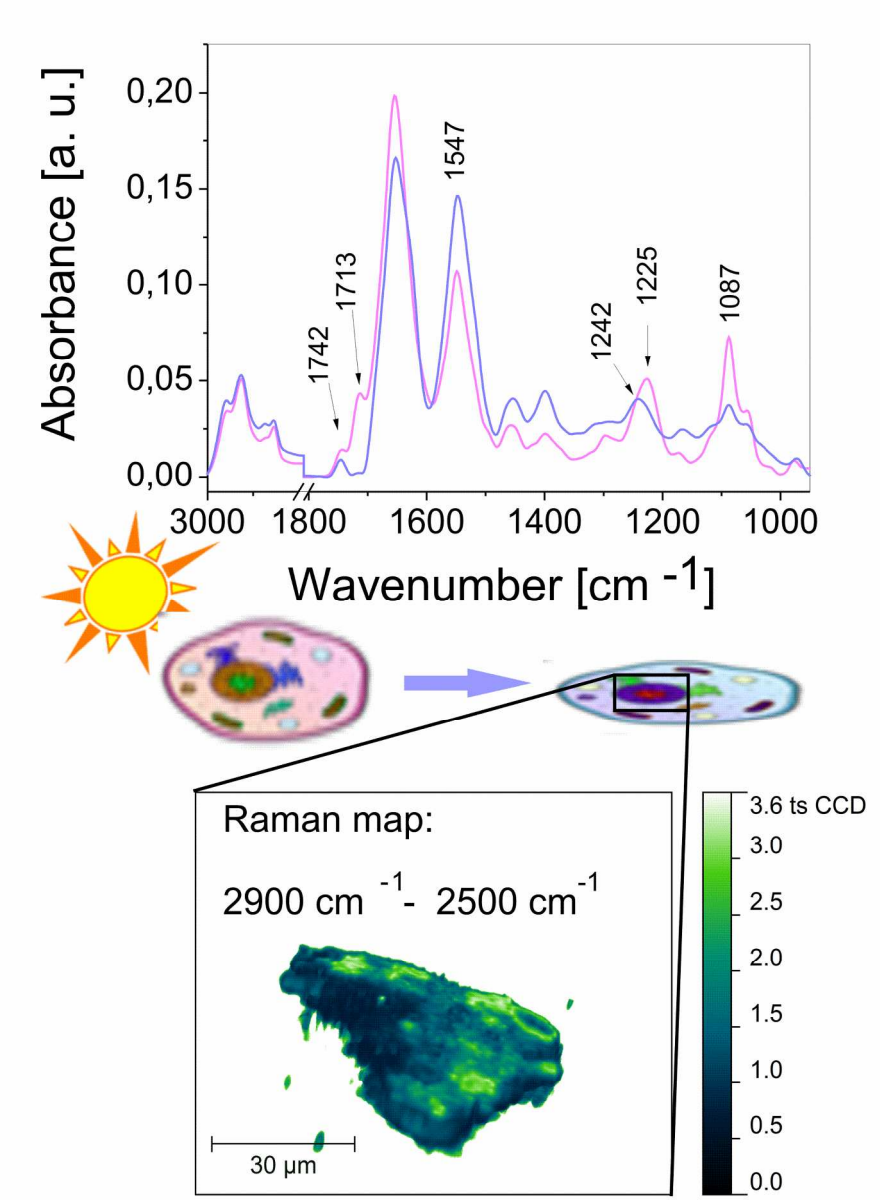

202x275mm (250 x 250 DPI)